

p-n Junction Based Direct-Current Triboelectric Nanogenerator by Conjunction of Tribovoltaic Effect and Photovoltaic Effect

Lele Ren, Aifang Yu, Wei Wang, Di Guo, Mengmeng Jia, Pengwen Guo, Yufei Zhang, Zhong Lin Wang,* and Junyi Zhai*



Cite This: <https://doi.org/10.1021/acs.nanolett.1c03922>



Read Online

ACCESS |



Metrics & More



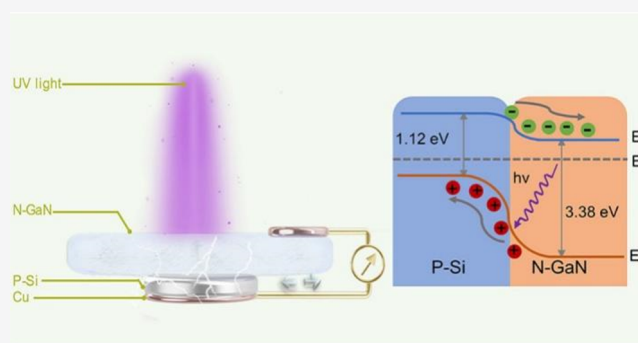
Article Recommendations



Supporting Information

ABSTRACT: Triboelectric nanogenerators (TENGs) have attracted much interest in recent years, due to its effectiveness and low cost for converting high-entropy mechanical energy into electric power. The traditional TENGs generate an alternating current, which requires a rectifier to provide a direct-current (DC) power supply. Herein, a dynamic p-n junction based direct-current triboelectric nanogenerator (DTENG) is demonstrated. When a p-Si wafer is sliding on a n-GaN wafer, carriers are generated at the interface and a DC current is produced along the direction of the built-in electric field, which is called the tribovoltaic effect. Simultaneously, an UV light is illuminated on the p-n junction to enhance the output. The results indicate that the current increases 13 times and the voltage increases 4 times under UV light (365 nm, 28 mW/cm²) irradiation. This work demonstrates the coupling between the tribovoltaic effect and the photovoltaic effect in DTENG semiconductors, promoting further development for energy harvesting in mechanical energy and photon energy.

KEYWORDS: direct current triboelectric nanogenerator, p-n junction, tribovoltaic effect, photovoltaic effect, energy harvesting, green energy



INTRODUCTION

With the fast development of human society, the demand for energy is expanding and must be distributed; thus, the attainment of sustainable energy from ambient sources is an important issue. Since the discovery of the contact electrification (CE) phenomenon 2600 years ago, converting mechanical energy into electricity has attracted much attention to achieve sustainable social development.^{1–4} More importantly, the rise of the Internet of things (IoTs) requires the energy supply to be miniaturized, to save energy, and to protect the environment.^{5–7} On this basis, the Wang group proposed the triboelectric nanogenerator (TENG) in the 2012, which utilized triboelectric effect and electrostatic induction to convert mechanical energy into electricity.⁸ From then on, TENG research expanded to a great number of application areas, such as self-powered systems, wearable devices, sensor devices, artificial intelligence, and so on.^{9–12} As most electronic devices are demand a direct current (DC) power supply, the traditional TENGs require a rectifier to convert AC into DC, which increases the complexity for the application of TENGs.^{13–15} In order to solve this problem, new TENGs have been developed to directly convert mechanical energy into DC, which are called direct current triboelectric nanogenerators (DTENGs). Wang et al. have combined the electrostatic breakdown with the triboelectrification effect to output constant DC.¹⁶

In addition, some previous works have paid attention to semiconductor-material-based DTENGs, including a metal–semiconductor Schottky contact, a p-n junction, a liquid–semiconductor contact, semiconductor homojunction, and so on.^{1,17–20} The semiconductor material could generate high density and DC output comparable to those of an organic polymer insulator material in TENGs, which have attracted much interest in semiconductor-based mechanical and electrical energy conversion and energy storage. Shao et al. first proposed DC output based on the Schottky contact of a polypyrrole (PPy) thin film and a metal electrode; the self-rectification of the Schottky barrier can achieve DC electricity.²¹ It has also been reported that sliding a Si atomic force microscope on a MoS₂ thin film can implement DC output; this causes the nanoscale tip friction to enhance the efficiency of the TENG.²² For dynamic p-n junctions, Xu et al. also proposed a direct current triboelectric cell by sliding p-Si and n-Si; this friction process stimulates the electrons and holes in the semiconductor, creating a built-in electric field to

Received: October 11, 2021

Revised: November 18, 2021

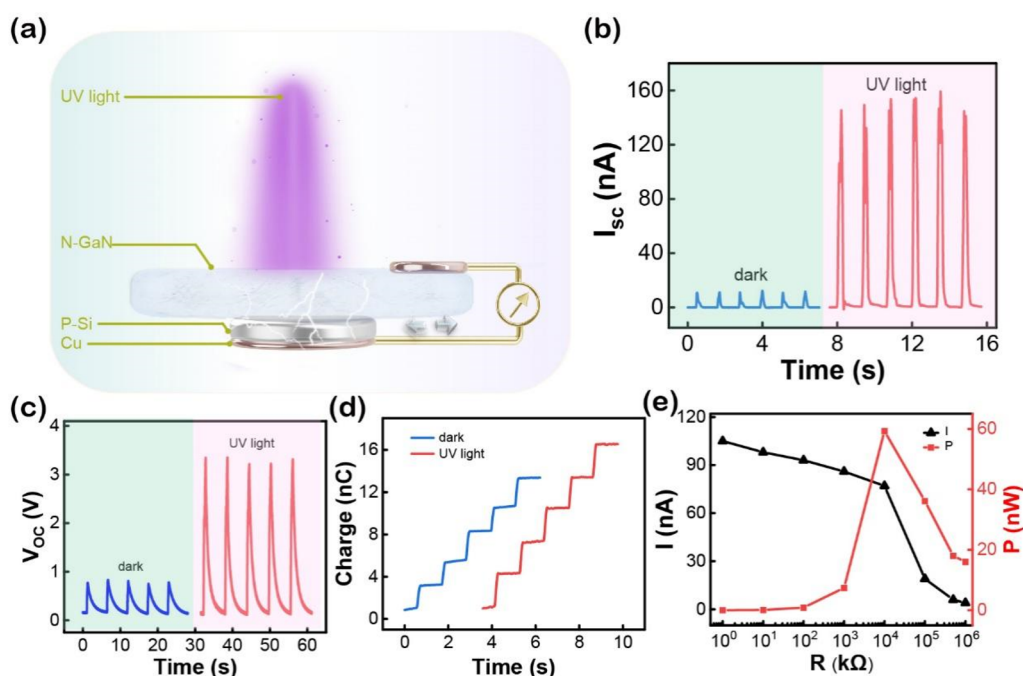


Figure 1. Experimental structure and the output of the p-n junction based direct-current triboelectric nanogenerator (DTENG) regulated by the UV light. (a) 3D schematic for the experimental setup. A p-Si slides on a n-GaN with the regulation of UV light. (b) I_{sc} , (c) V_{oc} , and (d) transferred charge of the DTENG in the dark and under UV light irradiation. (e) Output of current and power at the external load resistance of DTENG under UV light irradiation.

generate DC electricity.²³ The difference in the Fermi levels in the sliding p-n junction induces a potential difference and creates the voltage output. The DC excited by friction in semiconductor materials is due to the tribovoltaic effect.⁵ When the two semiconductor materials are rubbed against each other, the electron–hole pairs at the interface will be excited by the bindington, which is the energy quantum released when two atoms form a bond, and they will be separated by the built-in electric field, resulting in a DC current.^{24,25} This is called the tribovoltaic effect.⁵ Such a phenomenon is similar to the photovoltaic effect, all of which could excite electron–hole pairs and generate current along the direction of a built-in electric field. Some experiments have confirmed that the tribovoltaic effect and photovoltaic effect have a synergistic effect at a liquid–semiconductor interface and a metal–semiconductor interface.^{6,26,27} Therefore, the conjunction of the tribovoltaic effect and photovoltaic effect will improve the efficiency of energy harvesting.

Herein, we propose a p-n junction based DTENG modulated by ultraviolet (UV) light, where p-Si and n-GaN are chosen as the two friction layers. GaN is a wide-band-gap semiconductor with a band gap of approximately 3.4 eV, which has attracted a lot of interest because of the stationary absorption band for UV light, the high electron drift velocity, great chemical and mechanical stability.^{28,29} The p-Si is slid on the n-GaN without changing the contact area and is accompanied by generation of the DC. Due to the coupling of the tribovoltaic effect and photovoltaic effect, UV light can enhance the carrier concentration and increase the output of tribo-current and voltage. What is more, the higher optical power density, faster sliding speeds, larger resistivity of P–Si, and contact area of the p-n junction enhance the output of tribo-current and voltage. This work demonstrates that the tribovoltaic effect and photovoltaic effect can dramatically

enhance the energy output for the DTENG and offers a convenient method for promoting the DTENG to work as a self-powered system, an energy supply, and so on.

RESULTS AND DISCUSSION

For the DTENG based on a dynamic p-n junction, the detailed schematic structure is shown in Figure 1a. When the p-Si slides back and forth on the n-GaN surface, the electrons flow from the n-zone with a high Fermi level to the p-zone with a low Fermi level, forming a built-in electric field between n-GaN and p-Si and thus inducing a DC current in the external circuit.²² To investigate how the light modulates the output of the DTENG, a 365 nm UV light with a power density of 28 mW/cm² is illuminated from the n-GaN to the p-Si. Figure 1b,c demonstrate the short-circuit current (I_{sc}) and open-circuit voltage (V_{oc}) in the dark and under UV light irradiation with a sliding speed of 50 mm/s, respectively. The I_{sc} value is about 12 nA in the dark and 154 nA under UV light illumination, which increases by 1 order of magnitude upon the application of the light. Moreover, the V_{oc} value increases from 0.8 to 3.35 V when UV light is applied. The I_{sc} value increases more than the V_{oc} value with UV light illumination, which may be due to a decrease in the internal resistance at the p-n junction interface and the direct current being more sensitive to the concentration of carriers. Hence, with the UV light irradiation, the friction and photons simultaneously excite carriers, leading to an increase in the direct current and voltage. The voltage is determined by the strength of the built-in electric field, and the increase in voltage is limited when the electric field is high enough. More importantly, the continuous sliding could maintain the constant DC outputs (both I_{sc} and V_{oc}), as illustrated in Figure S1, no matter whether the sliding was in the dark or under UV light irradiation.

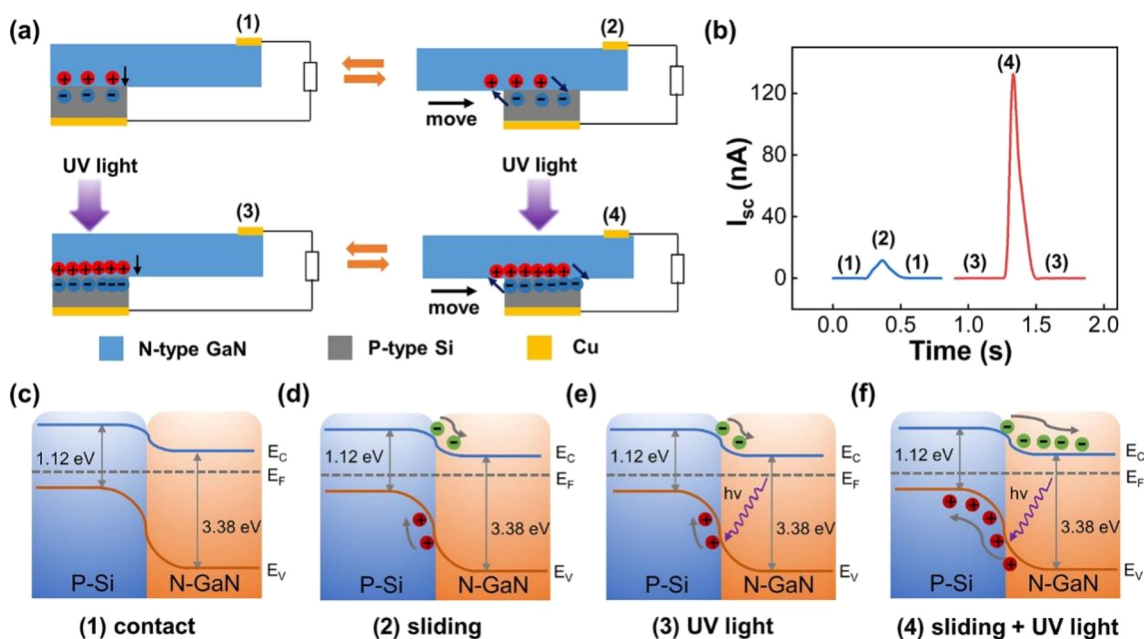


Figure 2. Working mechanism of the DTENG. (a) Working mechanism at (1) the connect still stage, (2) move to generate charges, (3) return to the still stage with UV light irradiation, and (4) reverse sliding to generate triboelectric charges with UV light irradiation. (b) Schematics of the I_{sc} of the DTENG in the dark and under UV light irradiation. The energy band diagrams of the p-n junction in (c) the contact stage, (d) the sliding stage, (e) the UV light irradiation stage, and (f) sliding with the UV light irradiation.

Furthermore, Figure 1d compares the output of charges with/without UV light irradiation (365 nm, 28 mW/cm²) at the same sliding speed, which indicates that the charge curve has a stepped-like shape due to the sliding back and forth at the same contact area and the transferred charge grows more quickly under the UV light irradiation. Figure 1e shows the external load resistance dependence of current and power under a constant sliding speed of 50 mm/s with UV light irradiation. The current decreases with an increase in the external load resistance. However, the power increases first and then decreases with the maximum power of approximately 60 nW at the load resistance of 10 M Ω . Simultaneously, the voltage increases with an increase of load resistance, as illustrated in Figure S2. In comparison to the dark, the UV light can obviously enhance the output of the current, voltage, and charge, which is interpreted as the UV light increasing the electron–hole pair concentration at the p-n junction interface.

To further understand the conjunction of the tribovoltatic effect and the photovoltaic effect on the dynamic p-n junction DTENG, the working mechanism and energy band structure are demonstrated. In Figure 2a, we first discuss such DTENG without UV irradiation; initially, the p-Si contacts n-GaN and keeps still as illustrated in the stage (1). When the p-Si slides on the n-GaN surface, the bindington could excite electron–hole pairs at the p-Si and n-GaN interface, which will move along the direction of the built-in electric field and generate DC, as shown in the stage (2). The stage (3) shows that when the p-Si stops at the end of the n-GaN and a UV light is applied on the p-n junction, the UV light will excite photoinduced carriers on the p-n junction, which dramatically increases the surface charge density on both of p-Si and n-GaN. When p-Si slides on the n-GaN with UV light irradiation as illustrated in the stage (4), the output performance of the direct current increases more in comparison with the stage (2) due to the increase in electron–hole pair concentration at the interface of the p-n junction. The pulsed current curves in

Figure 2b correspond to the different movement stages of the p-Si in Figure 2a.

The energy band diagrams of the p-n junction are illustrated in Figure 2c–f. When p-Si and n-GaN contact to form the p-n junction as shown in Figure 2c, the electrons flow from the n-zone with a high Fermi level to the p-zone with a low Fermi level, accompanied by the Fermi level of an n-type semiconductor (E_{Fn}) moving down and the Fermi level of p-type semiconductor (E_{Fp}) moving up to form the unified Fermi level in the p-n junction, and the conduction band and valence band in the p-zone and n-zone become bent. However, the electrons transitioning from the n-zone to the p-zone must cross a potential barrier, which is called the built-in potential, denoted V_{bi} . The potential barrier height compensates for the difference in Fermi level in the p and n regions, which can be described as

$$qV_{bi} = E_{Fn} - E_{Fp} \quad (1)$$

where q is the unit charge. Meanwhile, the equilibrium electron concentrations in the n region and p region are defined as

$$n_{n0} = n_i \exp[(E_{Fn} - E_i)/k_0T] \quad (2)$$

$$n_{p0} = n_i \exp[(E_{Fp} - E_i)/k_0T] \quad (3)$$

where n_i is the intrinsic carrier concentration, E_i is the intrinsic Fermi level, k_0 is the Boltzmann constant, and T is the temperature. Dividing eq 2 by eq 3 and taking the logarithm, we get

$$\ln(n_{n0}/n_{p0}) = (E_{Fn} - E_{Fp})/k_0T \quad (4)$$

$n_{n0} = N_D$ and $n_{p0} = n_i^2/N_A$; therefore, V_{bi} is given as

$$\begin{aligned} V_{bi} &= (E_{Fn} - E_{Fp})/q = \ln(n_{n0}/n_{p0})k_0T/q \\ &= (N_A N_D / n_i^2)k_0T/q \end{aligned} \quad (5)$$

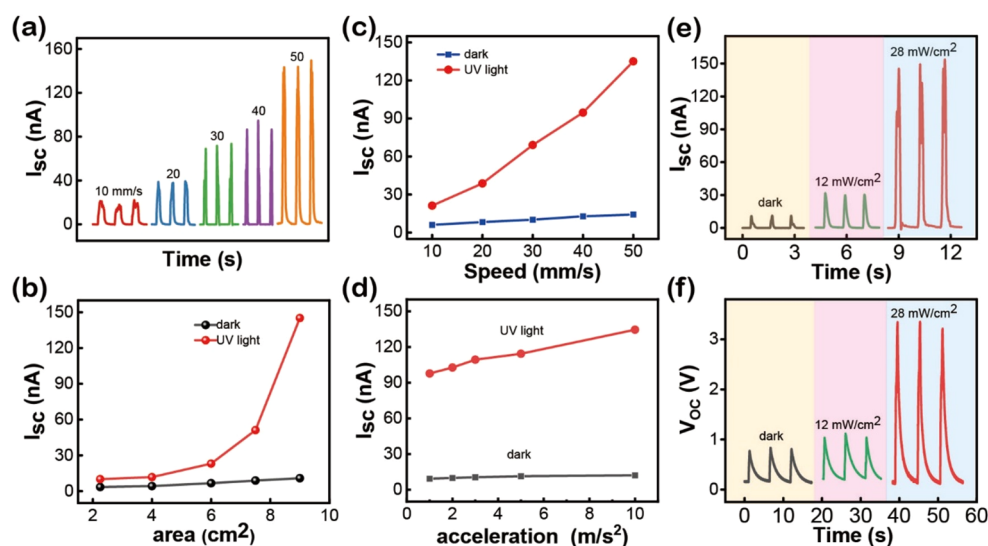


Figure 3. I_{sc} and V_{oc} of the DTENG at different sliding speeds, accelerations, contact areas, and optical power densities. (a) I_{sc} of the DTENG at different sliding speeds with the UV light irradiation. (b) I_{sc} against different contact areas of p-Si sliding on n-GaN in the dark and under UV light irradiation. (c) I_{sc} with different sliding speeds in the dark and under UV light irradiation. (d) I_{sc} with different accelerations in the dark and under UV light irradiation. (e) I_{sc} and (f) V_{oc} at different optical power densities of UV light.

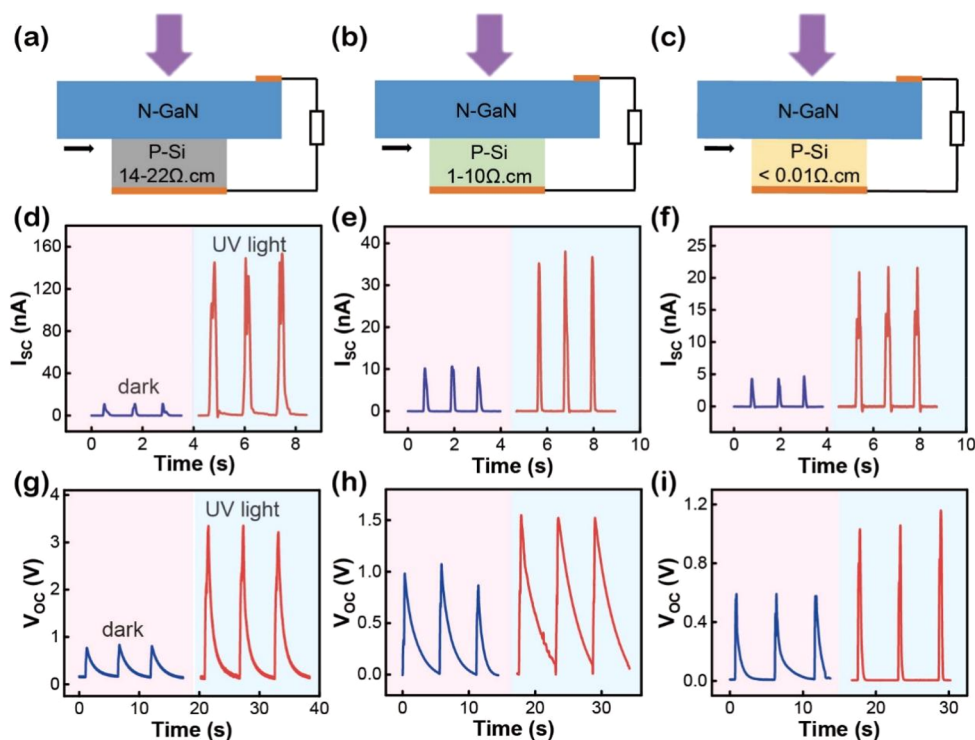


Figure 4. Influence of p-Si doping concentration on the output for the DTENG. (a–c) Schematic of n-GaN and p-Si with different resistivities. (d–f) I_{sc} output of p-Si with resistivities of 14–22 $\Omega\cdot\text{cm}$, 1–10 $\Omega\cdot\text{cm}$, and below 0.01 $\Omega\cdot\text{cm}$. (g–i) V_{oc} output of p-Si with resistivities of 14–22 $\Omega\cdot\text{cm}$, 1–10 $\Omega\cdot\text{cm}$, and below 0.01 $\Omega\cdot\text{cm}$.

where N_D is the donor concentration and N_A is the acceptor concentration. The formulas show that V_{bi} is related to the doping concentration, the temperature, and the band gap of the p–n junction.³⁰

When p-Si slides on n-GaN, the energy band diagram is shown in Figure 2d. During the sliding process, the thermal equilibrium in the p–n junction is disrupted and the mechanical energy converts into electrical energy and generates an external current. When the sliding process stops and a UV light is

applied to the p–n junction, the photon excites electron–hole pairs at the p–n junction interface, as indicated in Figure 2e. Moreover, Figure 2f exhibits the band structure of sliding with the UV light irradiation; the friction and photons stimulate more carriers at the p–n junction interface, resulting in a higher output of the current density, which also be called a majority carrier device.³¹ However, the discharging process of the p–n junction is unrelated to the sliding direction. We can conclude that the dynamic sliding process leads to the Fermi level of the

p-n junction in a nonequilibrium state; simultaneously, the barrier height changes in the interface and the movement of the carriers destroy the original balance, resulting in the potential difference and the output of direct voltage.

The effect of the sliding speeds, accelerations, optical power density, and contact area on the p-n based DTENG have been investigated. Figure 3a shows the I_{sc} value under UV light irradiation with sliding speeds from 10 to 50 mm/s. When the sliding speed increases from 10 to 50 mm/s, the I_{sc} value increases by around 6 times. Figure S4 shows the output of I_{sc} in the dark, and Figure 3c compares the output of I_{sc} in the dark and under UV light irradiation with an increase in the sliding speed from 10 to 50 mm/s. The output of V_{oc} changes with the sliding speed in the dark and under UV light irradiation is revealed in Figure S3. During the sliding process, the acceleration affects the generation of the current, as illustrated in Figure 3d. Thus, the regulation of the sliding speeds and accelerations for the DC output in the p-n junction is more obvious under UV light irradiation. This corresponds to the electron–hole pairs excited by the friction and photon being in the same direction, making the conjunction of the tribovoltage effect and photovoltaic effect. Furthermore, the relationship of DC performance and the contact area between p-Si and n-GaN are illustrated in Figure 3b and Figure S5. We select different areas of p-Si sliding on the n-GaN, indicating that the DC current and voltage output are positive to the contact area in the dark and under UV light irradiation. The dependence of I_{sc} and V_{oc} on optical power density are shown in Figure 3e,f, respectively. As the light intensity increases from 12 to 28 mW/cm², the I_{sc} value increases from 31 to 154 nA and the V_{oc} value increases from 1.11 to 3.35 V. The higher the light density, the more the electron–hole pairs are excited at the p-n junction interface, leading to the increase in I_{sc} and V_{oc} .

It is also seen that the doping concentration of p-Si influences the DC output, because of the difference in Fermi level at the p-n junction surface. As shown in Figure 4a–c, we selected p-Si with different resistances sliding on the n-GaN, which are 14–22 Ω·cm, 1–10 Ω·cm, and below 0.01 Ω·cm. The I_{sc} and V_{oc} values are shown in Figure 4d–f and Figure 4g–i, respectively. The results indicate that p-Si with a higher resistivity produces a higher DC output, especially under UV light irradiation. What is more, the resistivity of p-Si is determined by the doping concentration: the higher the doping concentration, the lower the resistivity. In the extrinsic semiconductor, doping of donor or acceptor impurity atoms will change the distribution of electrons and holes. In addition, the Fermi level is related to the distribution function, and it will change with the electron concentration in the conduction band and the hole concentration in the valence band.³²

For the semiconductor in a thermal equilibrium, the electron and hole concentrations are defined as

$$n_0 = N_c \exp[-(E_c - E_F)/k_0T] \quad (6)$$

$$p_0 = N_v \exp[-(E_F - E_v)/k_0T] \quad (7)$$

where N_c is the effective state density of the conduction band, N_v is the effective state density of the valence band, E_F is the Fermi level, E_c is the bottom of the conduction, E_v is the top of the valence band, k_0 is the Boltzmann constant, and T is the absolute temperature. With regard to the p-type semiconductor, the hole concentration is defined as $p_0 = N_A$, where N_A is the acceptor concentration. It can be calculated from the above formula.³⁰

$$E_F - E_v = k_0T \ln(N_v/N_A) \quad (8)$$

The higher the acceptor concentration, the smaller the energy difference ($E_F - E_v$), and the Fermi level is closer to the top of the valence band. On the whole, the barrier height of the p-n junction increases with the doping concentration of p-Si. Simultaneously, the electron and hole transitions in the p-n junction will step across a high barrier height. When p-Si slides on n-GaN, the barrier height decreases with an increase in p-Si resistance, which also increases the carrier concentration in the interface, leading to more carrier transfer between p-Si and n-GaN and an increase in the DC output. Furthermore, the UV light also excites carriers at the interface: the lower the barrier height, the more the carriers can be excited. This is illustrated from Figure S6, where p-Si with high resistance results in the DC output being obviously enhanced under the UV light irradiation.

In order to explore the photon effect for the DTENG properties, we measured the electrical performance of the p-Si and n-GaN based p-n junction. The schematic structure of the Si/GaN p-n junction is indicated in Figure 5a; the UV light stimulates the photogenerated carriers at the interface, bringing about the photoresponse in the p-n junction. Figure 5b gives the I – V curve of the p-n junction in the dark and under UV light (365 nm, 28 mW/cm²) irradiation. The photocurrent is

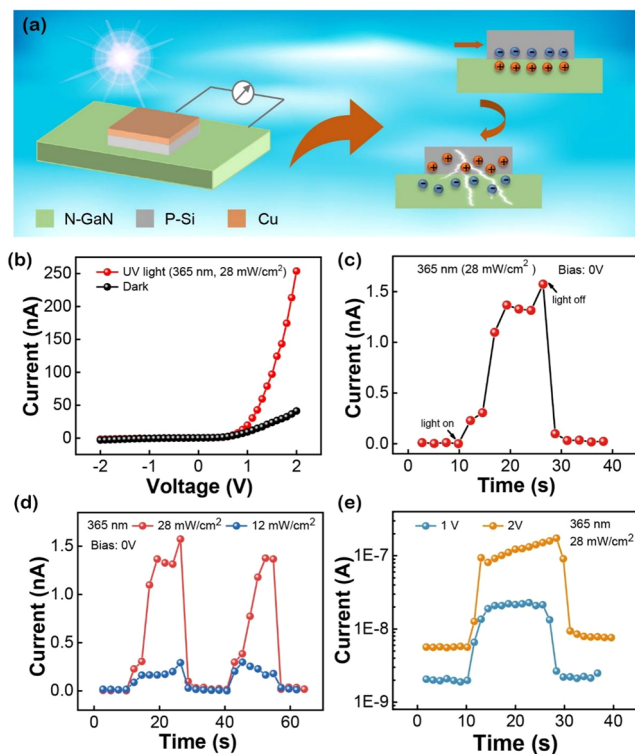


Figure 5. Photoelectric properties of the Si/GaN p-n junction. (a) Schematic of the Si/GaN p-n junction, producing photogenerated carriers at the interface with the UV light irradiation. (b) I – V property curve of the p-n junction in the dark and under UV light (365 nm, 28 mW/cm²) irradiation. (c) Time-dependent current of the p-n junction with a 365 nm UV light irradiation of 28 mW/cm² under zero bias. (d) Time-dependent current of the p-n junction toward 365 nm light irradiation with light intensities of 28 and 12 mW/cm² at zero bias. (e) Time-dependent current of the p-n junction under biases of 1 and 2 V with 365 nm UV light (28 mW/cm²) illumination.

weak under the negative bias, while it is significantly enhanced under the positive bias, which indicates the typical rectifying characteristics of the p-n junction. Under UV light irradiation, the photocurrent increases rapidly at the positive bias, demonstrating a prominent photoelectric conversion ability.³³ This also indicates that the p-n junction based on p-Si and n-GaN has a great diode function. Figure 5c shows the time-dependent current of the p-n junction by intermittently turning on and off the 365 nm UV light of 28 mW/cm² under a zero bias. It can be seen that the current is zero in the dark and increases to 1.5 nA when the UV light is turned on. Meanwhile the current stays at around 1.5 nA when the UV light continues to illuminate and will drop to zero when the UV light is turned off. The time-dependent current of the p-n junction at different optical power densities is illustrated in Figure 5d. As the light intensity increases from 12 to 28 mW/cm², the photocurrent increases from 0.2 to 1.5 nA, which shows that the light intensity can significantly enhance the switching performance of this p-n junction. Moreover, the photocurrent barely changes at the fixed light intensity, indicating that the photoresponse of the p-n junction has good repeatability.

We also investigated the bias voltage dependence of the photoresponse of the p-n junction, as shown in Figure 5e. As the bias increases from 1 to 2 V, the current increases from 2 to 5.6 nA in the dark, and the photocurrent rapidly increases from 22 to 120 nA. The *I*-*V* curve and time-dependent current of the p-n junction were all measured at the stationary state. In addition, the photocurrent we measured is relatively low and unstable. This is due to the p-Si and n-GaN in the p-n junction being formed in the contact way rather than by epitaxial growth of one material directly on top of the other. By measurement of the photoresponse curve of the p-n junction, the conclusion indicates that the UV light generates the photogenerated electron-hole pairs, which separate and diffuse under the drive of the built-in electric field in the depletion layer. In addition, the electrons transport toward p-Si and n-GaN to generate the photocurrent. Therefore, the tribovoltaic current and voltage apparently increase under the UV light irradiation. On the basis of the coupling of the tribovoltaic effect and photovoltaic effect, this DTENG can realize the coharvesting of solar energy and mechanical energy in various environments.

CONCLUSION

In conclusion, we have demonstrated a p-Si and n-GaN based DTENG regulated by the tribovoltaic effect and photovoltaic effect. The results confirm that the bindington could excite electron-hole pairs at the p-n junction interface and induce a built-in electric field, which generates a direct current in the external circuit. Simultaneously, the UV light could excite photogenerated carriers, which increases the concentration of electron-hole pairs in the p-n junction and leads to a significant increase in the direct current and voltage under the UV light irradiation. It turns out that the *I*_{sc} value is 154 nA and the *V*_{oc} value is 3.35 V under the UV light irradiation, increasing separately about 13 times and 4 times in contrast to those in the dark. In addition, the maximum power is approximately 60 nW under the UV light irradiation. Moreover, the output performance of the DTENG increases by sliding speeds, optical power densities, accelerations, contact areas, and resistivities of p-Si. Our work verifies the synergistic effect of the tribovoltaic effect and photovoltaic effect, opening up new ideas to harvest energy in semiconductor materials. These

findings will also promote triboelectric applications in semiconductor devices and photoelectronic devices.

ASSOCIATED CONTENT

Supporting Information

The Supporting Information is available free of charge at <https://pubs.acs.org/doi/10.1021/acs.nanolett.1c03922>.

Experimental section and additional figures (PDF)

AUTHOR INFORMATION

Corresponding Authors

Zhong Lin Wang – CAS Center for Excellence in Nanoscience, Beijing Key Laboratory of Micro-nano Energy and Sensor, Beijing Institute of Nanoenergy and Nanosystems, Chinese Academy of Sciences, Beijing 100083, People's Republic of China; College of Nanoscience and Technology, University of Chinese Academy of Sciences, Beijing 100049, People's Republic of China; School of Materials Science and Engineering, Georgia Institute of Technology, Atlanta, Georgia 30332, United States; orcid.org/0000-0002-5530-0380; Email: zlwang@gatech.edu

Junyi Zhai – CAS Center for Excellence in Nanoscience, Beijing Key Laboratory of Micro-nano Energy and Sensor, Beijing Institute of Nanoenergy and Nanosystems, Chinese Academy of Sciences, Beijing 100083, People's Republic of China; College of Nanoscience and Technology, University of Chinese Academy of Sciences, Beijing 100049, People's Republic of China; Center on Nanoenergy Research, School of Physical Science and Technology, Guangxi University, Nanning 530004, People's Republic of China; orcid.org/0000-0001-8900-4638; Email: jyzhai@binn.cas.cn

Authors

Lele Ren – CAS Center for Excellence in Nanoscience, Beijing Key Laboratory of Micro-nano Energy and Sensor, Beijing Institute of Nanoenergy and Nanosystems, Chinese Academy of Sciences, Beijing 100083, People's Republic of China; College of Nanoscience and Technology, University of Chinese Academy of Sciences, Beijing 100049, People's Republic of China

Aifang Yu – CAS Center for Excellence in Nanoscience, Beijing Key Laboratory of Micro-nano Energy and Sensor, Beijing Institute of Nanoenergy and Nanosystems, Chinese Academy of Sciences, Beijing 100083, People's Republic of China; College of Nanoscience and Technology, University of Chinese Academy of Sciences, Beijing 100049, People's Republic of China; Center on Nanoenergy Research, School of Physical Science and Technology, Guangxi University, Nanning 530004, People's Republic of China

Wei Wang – CAS Center for Excellence in Nanoscience, Beijing Key Laboratory of Micro-nano Energy and Sensor, Beijing Institute of Nanoenergy and Nanosystems, Chinese Academy of Sciences, Beijing 100083, People's Republic of China; College of Nanoscience and Technology, University of Chinese Academy of Sciences, Beijing 100049, People's Republic of China

Di Guo – CAS Center for Excellence in Nanoscience, Beijing Key Laboratory of Micro-nano Energy and Sensor, Beijing Institute of Nanoenergy and Nanosystems, Chinese Academy of Sciences, Beijing 100083, People's Republic of China; Center on Nanoenergy Research, School of Physical Science

and Technology, Guangxi University, Nanning 530004, People's Republic of China

Mengmeng Jia – CAS Center for Excellence in Nanoscience, Beijing Key Laboratory of Micro-nano Energy and Sensor, Beijing Institute of Nanoenergy and Nanosystems, Chinese Academy of Sciences, Beijing 100083, People's Republic of China; College of Nanoscience and Technology, University of Chinese Academy of Sciences, Beijing 100049, People's Republic of China

Pengwen Guo – CAS Center for Excellence in Nanoscience, Beijing Key Laboratory of Micro-nano Energy and Sensor, Beijing Institute of Nanoenergy and Nanosystems, Chinese Academy of Sciences, Beijing 100083, People's Republic of China; College of Nanoscience and Technology, University of Chinese Academy of Sciences, Beijing 100049, People's Republic of China

Yufei Zhang – CAS Center for Excellence in Nanoscience, Beijing Key Laboratory of Micro-nano Energy and Sensor, Beijing Institute of Nanoenergy and Nanosystems, Chinese Academy of Sciences, Beijing 100083, People's Republic of China; College of Nanoscience and Technology, University of Chinese Academy of Sciences, Beijing 100049, People's Republic of China

Complete contact information is available at:

<https://pubs.acs.org/10.1021/acs.nanolett.1c03922>

Author Contributions

Z.L.W. and J.Z. conceived and led this project. L.R. performed all of the experiments. A.Y., W.W., and D.G. helped with the analysis of experimental results. M.J., P.G., and Y.Z. helped with the data analysis. All of the authors discussed the results and contributed to the manuscript preparation.

Notes

The authors declare no competing financial interest.

ACKNOWLEDGMENTS

This work was supported by the National Nature Science Foundation of China (Grant Nos. 52073032, 51872031, and 61904013) and the Fundamental Research Funds for the Central Universities.

REFERENCES

- (1) Lu, Y.; Gao, Q.; Yu, X.; Zheng, H.; Shen, R.; Hao, Z.; Yan, Y.; Zhang, P.; Wen, Y.; Yang, G.; Lin, S. Interfacial Built-In Electric Field-Driven Direct Current Generator Based on Dynamic Silicon Homo Junction. *Research* **2020**, *2020*, 5714754.
- (2) Zhong, H. K.; Xia, J.; Wang, F. C.; Chen, H. S.; Wu, H. A.; Lin, S. S. Graphene-Piezoelectric Material Heterostructure for Harvesting Energy from Water Flow. *Adv. Funct. Mater.* **2017**, *27*, 1604226.
- (3) Wang, S. H.; Lin, L.; Wang, Z. L. Triboelectric nanogenerators as self-powered active sensors. *Nano Energy* **2015**, *11*, 436–462.
- (4) Niu, S. M.; Wang, X. F.; Yi, F.; Zhou, Y. S.; Wang, Z. L. A universal self-charging system driven by random biomechanical energy for sustainable operation of mobile electronics. *Nat. Commun.* **2015**, *6*, 8975.
- (5) Wang, Z. L.; Wang, A. C. On the origin of contact-electrification. *Mater. Today* **2019**, *30*, 34–51.
- (6) Zheng, M.; Lin, S.; Tang, Z.; Feng, Y.; Wang, Z. L. Photovoltaic effect and tribovoltaic effect at liquid-semiconductor interface. *Nano Energy* **2021**, *83*, 105810.
- (7) Lowell, J.; Rose-Innes, A. C. Contact electrification. *Adv. Phys.* **1980**, *29* (6), 947–1023.
- (8) Fan, F.-R.; Tian, Z.-Q.; Lin Wang, Z. Flexible triboelectric generator. *Nano Energy* **2012**, *1* (2), 328–334.
- (9) Jiang, P.; Zhang, L.; Guo, H.; Chen, C.; Wu, C.; Zhang, S.; Wang, Z. L. Signal Output of Triboelectric Nanogenerator at Oil-Water-Solid Multiphase Interfaces and its Application for Dual-Signal Chemical Sensing. *Adv. Mater.* **2019**, *31* (39), 1902793.
- (10) Li, C.; Yin, Y.; Wang, B.; Zhou, T.; Wang, J.; Luo, J.; Tang, W.; Cao, R.; Yuan, Z.; Li, N.; Du, X.; Wang, C.; Zhao, S.; Liu, Y.; Wang, Z. L. Self-Powered Electrospinning System Driven by a Triboelectric Nanogenerator. *ACS Nano* **2017**, *11* (10), 10439–10445.
- (11) Sun, Q. J.; Zhao, X. H.; Yeung, C. C.; Tian, Q.; Kong, K. W.; Wu, W.; Venkatesh, S.; Li, W. J.; Roy, V. A. L. Bioinspired, Self-Powered, and Highly Sensitive Electronic Skin for Sensing Static and Dynamic Pressures. *ACS Appl. Mater. Interfaces* **2020**, *12* (33), 37239–37247.
- (12) Zhang, D.; Shi, J.; Si, Y.; Li, T. Multi-grating triboelectric nanogenerator for harvesting low-frequency ocean wave energy. *Nano Energy* **2019**, *61*, 132–140.
- (13) Zhang, C.; Zhou, T.; Tang, W.; Han, C.; Zhang, L.; Wang, Z. L. Rotating-Disk-Based Direct-Current Triboelectric Nanogenerator. *Adv. Energy Mater.* **2014**, *4* (9), 1301798.
- (14) Yang, Y.; Zhang, H.; Wang, Z. L. Direct-Current Triboelectric Generator. *Adv. Funct. Mater.* **2014**, *24* (24), 3745–3750.
- (15) Zhou, L.; Liu, D.; Li, S.; Yin, X.; Zhang, C.; Li, X.; Zhang, C.; Zhang, W.; Cao, X.; Wang, J.; Wang, Z. L. Effective removing of hexavalent chromium from wasted water by triboelectric nanogenerator driven self-powered electrochemical system – Why pulsed DC is better than continuous DC? *Nano Energy* **2019**, *64*, 103915.
- (16) Liu, D.; Yin, X.; Guo, H. Y.; Zhou, L. L.; Li, X. Y.; Zhang, C. L.; Wang, J.; Wang, Z. L. A constant current triboelectric nanogenerator arising from electrostatic breakdown. *Sci. Adv.* **2019**, *5* (4), eaav6437.
- (17) Hao, Z.; Jiang, T.; Lu, Y.; Feng, S.; Shen, R.; Yao, T.; Yan, Y.; Yang, Y.; Lu, Y.; Lin, S. Co-harvesting Light and Mechanical Energy Based on Dynamic Metal/Perovskite Schottky Junction. *Matter* **2019**, *1* (3), 639–649.
- (18) Lin, S.; Lu, Y.; Feng, S.; Hao, Z.; Yan, Y. A High Current Density Direct-Current Generator Based on a Moving van der Waals Schottky Diode. *Adv. Mater.* **2018**, *31* (7), 1804398.
- (19) Lu, Y.; Hao, Z.; Feng, S.; Shen, R.; Yan, Y.; Lin, S. Direct-Current Generator Based on Dynamic PN Junctions with the Designed Voltage Output. *iScience* **2019**, *22*, 58–69.
- (20) Liu, J.; Jiang, K.; Nguyen, L.; Li, Z.; Thundat, T. Interfacial friction-induced electronic excitation mechanism for tribo-tunneling current generation. *Mater. Horiz.* **2019**, *6* (5), 1020–1026.
- (21) Shao, H.; Fang, J.; Wang, H. X.; Zhou, H.; Lin, T. Direct current energy generators from a conducting polymer-inorganic oxide junction. *J. Mater. Chem. A* **2017**, *5* (18), 8267–8273.
- (22) Liu, J.; Goswami, A.; Jiang, K.; Khan, F.; Kim, S.; McGee, R.; Li, Z.; Hu, Z.; Lee, J.; Thundat, T. Direct-current triboelectricity generation by a sliding Schottky nanocontact on MoS₂ multilayers. *Nat. Nanotechnol.* **2018**, *13* (2), 112–116.
- (23) Xu, R.; Zhang, Q.; Wang, J. Y.; Liu, D.; Wang, J.; Wang, Z. L. Direct current triboelectric cell by sliding an n-type semiconductor on a p-type semiconductor. *Nano Energy* **2019**, *66*, 104185.
- (24) Zheng, M. L.; Lin, S. Q.; Xu, L.; Zhu, L. P.; Wang, Z. L. Scanning Probing of the Tribovoltaic Effect at the Sliding Interface of Two Semiconductors. *Adv. Mater.* **2020**, *32* (21), 2000928.
- (25) Zhang, Z.; He, T.; Zhao, J.; Liu, G.; Wang, Z. L.; Zhang, C. Tribo-thermoelectric and tribovoltaic coupling effect at metal-semiconductor interface. *Mater. Today Phys.* **2021**, *16*, 100295.
- (26) Tao, X.; Nie, J.; Li, S.; Shi, Y.; Lin, S.; Chen, X.; Wang, Z. L. Effect of Photo-Excitation on Contact Electrification at Liquid-Solid Interface. *ACS Nano* **2021**, *15* (6), 10609–10617.
- (27) Liu, J.; Zhang, Y.; Chen, J.; Bao, R.; Jiang, K.; Khan, F.; Goswami, A.; Li, Z.; Liu, F.; Feng, K.; Luo, J.; Thundat, T. Separation and Quantum Tunneling of Photo-generated Carriers Using a Tribo-Induced Field. *Matter* **2019**, *1* (3), 650–660.
- (28) Bockowski, M.; Iwinska, M.; Amilusk, M.; Fijalkowski, M.; Lucznik, B.; Sochacki, T. Challenges and future perspectives in HVPE-GaN growth on ammonothermal GaN seeds. *Semicond. Sci. Technol.* **2016**, *31* (9), 093002.

(29) Bie, Y. Q.; Liao, Z. M.; Zhang, H. Z.; Li, G. R.; Ye, Y.; Zhou, Y. B.; Xu, J.; Qin, Z. X.; Dai, L.; Yu, D. P. Self-powered, ultrafast, visible-blind UV detection and optical logical operation based on ZnO/GaN nanoscale p–n junctions. *Adv. Mater.* **2011**, *23* (5), 649–53.

(30) Sze, S. M.; Ng, K. K. *Physics of semiconductor devices*, 3rd ed.; Wiley-Interscience: 2007.

(31) Wang, Z. L. On Maxwell's displacement current for energy and sensors: the origin of nanogenerators. *Mater. Today* **2017**, *20* (2), 74–82.

(32) Liu, J.; Liu, F.; Bao, R.; Jiang, K.; Khan, F.; Li, Z.; Peng, H.; Chen, J.; Alodhayb, A.; Thundat, T. Scaled-up Direct-Current Generation in MoS₂Multilayer-Based Moving Heterojunctions. *ACS Appl. Mater. Interfaces* **2019**, *11* (38), 35404–35409.

(33) Guo, D.; Su, Y.; Shi, H.; Li, P.; Zhao, N.; Ye, J.; Wang, S.; Liu, A.; Chen, Z.; Li, C.; Tang, W. Self-Powered Ultraviolet Photodetector with Superhigh Photoresponsivity (3.05 A/W) Based on the GaN/Sn:Ga₂O₃ pn Junction. *ACS Nano* **2018**, *12* (12), 12827–12835.